

Charge Order and Fluctuations in $\text{Bi}_2\text{Sr}_{2-x}\text{La}_x\text{CuO}_{6+\delta}$ Revealed by $^{63,65}\text{Cu}$ -Nuclear Magnetic Resonance

Shinji Kawasaki,¹ Madoka Ito,¹ Dai Kamijima,¹ Chengtian Lin,² and Guo-qing Zheng¹

¹*Department of Physics, Okayama University, Okayama 700-8530, Japan*

²*Max-Planck-Institut für Festkörperforschung, Heisenbergstrasse 1, D-70569 Stuttgart, Germany*

The discovery of a magnetic-field-induced charge-density-wave (CDW) order in the pseudogap state via nuclear magnetic resonance (NMR) studies has highlighted the importance of “charge” in the physics of high transition-temperature (T_c) superconductivity in copper oxides (cuprates). Herein, after briefly reviewing the progress achieved in the last few years, we report new results of $^{63,65}\text{Cu}$ -NMR measurements on the CDW order and its fluctuation in the single-layered cuprate $\text{Bi}_2\text{Sr}_{2-x}\text{La}_x\text{CuO}_{6+\delta}$. The NMR spectrum under both in- and out-of-plane magnetic fields above $H = 10$ T indicates that the CDW replaces the antiferromagnetic order before superconductivity appears, but disappears before superconductivity is optimized. We found that the CDW onset temperature T_{CDW} scales with the pseudogap temperature T^* . Comparison between ^{63}Cu and ^{65}Cu NMR indicates that the spin-lattice relaxation process is dominated by charge fluctuations in the doping regions where the CDW appears as well as at the pseudogap end point ($T^* = 0$). These results suggest that charge orders and fluctuations exist in multiple doping regions and over a quite wide temperature range.

I. INTRODUCTION

Since the discovery of superconductivity in $\text{La}_{2-x}\text{Ba}_x\text{CuO}_4$ in 1986¹, copper oxide (cuprate) has been thoroughly investigated towards a realization of room-temperature superconductivity². One of the remarkable features of cuprate superconductivity is its Cooper pair symmetry, which has been established to be an anisotropic d -wave gap with spin singlet³. This is a manifestation of strong electron correlations in contrast to the electron phonon interaction in conventional superconductors⁴. Unfortunately, the superconducting transition temperature (T_c) did not increase after the discovery of $T_c = 134$ K in $\text{HgBa}_2\text{Ca}_2\text{Cu}_3\text{O}_{8+\delta}$ in 1993⁵. The mechanism of superconductivity remains unclear as well, although it is well accepted that it is tightly related to Mott insulating phase⁶.

Among others, the “pseudogap” phenomenon is an unsettled issue⁷, first found by nuclear magnetic resonance (NMR) experiments^{8,9}. The nuclear spin-lattice relaxation rate divided by the temperature $1/T_1T$ and Knight shift (K) decreases below a certain temperature (hereafter referred as T^*). This indicates that the density of states (DOS) is reduced below T^* which is above an antiferromagnetic transition or T_c ^{8–11}. The angle-resolved photoemission spectroscopy (ARPES) experiments have shown that the pseudogap opens around $(\pi, 0)$ region in the momentum space below T^* above T_c , whose momentum dependence closely resembles that of the $d_{x^2-y^2}$ gap observed in the superconducting state^{12–14}. Thus, the focus has been on the relationship between the pseudogap and the superconducting gap¹⁵. Regarding this, we have performed NMR measurements on single-layered $\text{Bi}_2\text{Sr}_{2-x}\text{La}_x\text{CuO}_{6+\delta}$ (Bi2201) superconductors after suppressing superconductivity by strong magnetic field and revealed that the two gaps are co-existing matter^{10,11}. However, the cause for the DOS

decrease below T^* is still unclear.

Combining ARPES, polar Kerr effect, and time-resolved reflectivity experiments in Bi2201, it was argued that T^* is associated with a phase transition to a symmetry-broken state¹⁶. On the other hand, previous NMR experiments found no internal magnetic field due to magnetic order^{11,17,18} nor C_4 symmetry breaking below T^* ¹⁹. Although a unified understanding of the origin of the pseudogap has not been reached, some clues have been obtained. In La-based cuprates, at hole concentration $p = 1/8$, neutron scattering measurements have found a “stripe” phase due to the spin/charge order that competes with superconductivity^{20–22}. Indeed, when a strong magnetic field is applied to $\text{YBa}_2\text{Cu}_3\text{O}_y$ (YBCO) to suppress superconductivity, a long range ordered charge density wave (CDW) shows up²³. The field-induced CDW is not limited to YBCO, but also found in Bi2201²⁴, although the relationship between CDW and superconductivity is quite different among the two classes of compounds. In the former case, the CDW arises only from the mixed state around $p = 1/8$ ²³, but in the latter case it appears above T_c to take over antiferromagnetism, coexisting with superconductivity and disappearing before superconductivity reaches optimum²⁴. Furthermore, scanning tunneling microscopy (STM) of $\text{Bi}_2\text{Sr}_2\text{CaCu}_2\text{O}_{8+\delta}$ (Bi2212) revealed a modulation of the local DOS in the vortex cores²⁵, which was interpreted as a result of incipient charge order localized within the vortex halos^{26,27}. In that region, a pair density wave (PDW) order in which the order parameter varies periodically in space has been proposed²⁸. These results suggest that multiple orders are intertwined in the pseudogap region, and “density wave” has become a hot topic^{29–31}.

The rest of this article is organized as follows. In Section 2, we review CDWs observed in cuprates mainly from an NMR point of view. In Sections 3, we report new results of CDW order and fluctuations obtained through $^{63,65}\text{Cu}$ -NMR measurements on Bi2201. In section 4, we

discuss the results in connection to other orders such as nematic order and possible quantum criticality associated with pseudogap end point, before summarizing in Section 5.

II. REVIEW OF CDWS IN CUPRATES

The discovery of a magnetic field-induced CDW order in YBCO²³ highlights the importance of “charge”. Thus far, the CDW order has been confirmed only in YBCO^{23,32,33} and Bi2201²⁴. We review the current status of the CDW studies in this section.

A. Magnetic field induced CDW order

In 2011, Wu *et al* discovered a magnetic-field-induced CDW order in underdoped YBCO [Fig. 1(a)]²³. According to their results, a CDW appears inside the superconducting dome in a field perpendicular to the CuO₂ plane ($H \parallel c$) above $H = 15$ T, but not in a parallel field ($H \perp c$)²³. The transition temperature (T_{CDW}) is the highest at approximately $p = 1/8$, but lower than the zero-field T_c [$T_{CDW} \leq T_c (H = 0)$]³⁴. In contrast, as seen in Fig. 1(b), the onset field of the CDW (H_{CDW}) at $T = 0$ scales with the upper critical field H_{c2} and is the smallest at $p = 1/8$ ³⁴. Further, the fact that the superconductivity is inherently suppressed at $p = 1/8$, where the CDW is likely to be induced, suggests that the CDW and superconductivity are competing orders²³. From these results, it was suggested that the CDW may develop owing to an overlap of the local charge density modulation at the vortex center²⁵ in the mixed state³⁴.

Following the experiments on YBCO, high-field NMR experiments were performed in HgBa₂CuO_{4+ δ} (Hg1201)³⁵. No evidence for field- or temperature-induced spin/charge order was found nor was there any correlation with the vortex or with the pseudogap. Therefore, it was concluded that field-induced CDWs are absent in Hg1201³⁵.

In 2017, we reported high-field NMR measurements up to $H = 45$ T in single-layered Bi2201 superconductors and discovered CDWs induced by an *in-plane* magnetic field $H \perp c$ ²⁴. As shown in Figs. 1(a)-(d), the doping dependence of the CDW and its relation to superconductivity are different in YBCO and Bi2201. The CDW of Bi2201 appears above T_c to replace the antiferromagnetic order. Furthermore, although T_{CDW} is of the same order in both compounds, H_{CDW} and T_{CDW} seem to be related to the doping level itself in Bi2201, but not to H_{c2} or superconductivity. Thus, the CDW in Bi2201 is more likely to be induced near the antiferromagnetic order than at the specific hole concentration $p = 1/8$. This difference is also observed in high-temperature CDW correlations. Next, we briefly review the normal state properties.

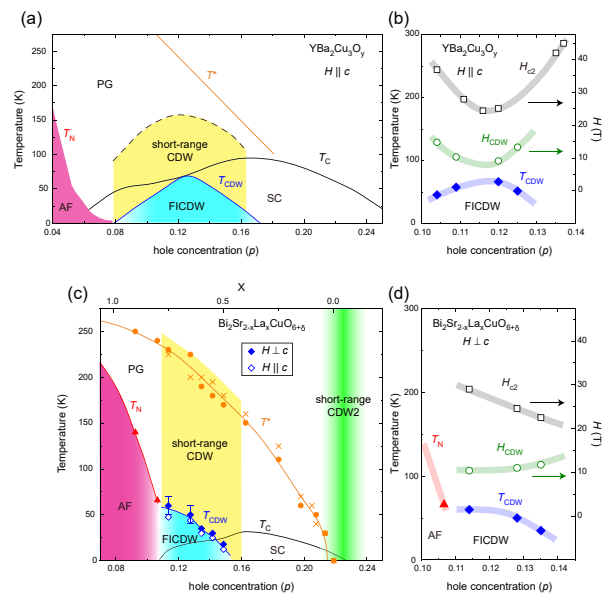


Fig. 1: Doping dependence of short-range CDW/CDW2^{2,41,42,46}, field-induced CDW (FICDW), and its relation to upper critical field (H_{c2}) and the onset field H_{CDW} for YBa₂Cu₃O_y (a), (b) and Bi₂Sr_{2-x}La_xCuO_{6+ δ} (c), (d). For both cases, T_c is the zero-field value. The schematic phase diagram for YBa₂Cu₃O_y is from the literatures^{2,23,34}.

B. CDW correlation length

After the aforementioned NMR study²³, resonant X-ray scattering (RXS) experiments on YBCO at $H = 0$ have revealed an in-plane short-range CDW [Fig. 1(a)] with wave vector $\mathbf{Q} = (\sim 0.3, 0)$, $(0, \sim 0.3)$, and correlation lengths $\xi_{a,b} \sim 50 \text{ \AA}$ ^{36,37}. The CDW appears below T^* , but is suppressed below T_c ^{36,37}. The onset temperature of the CDW is consistent with a peak in $1/T_1 T$ ³⁸ and has a similar doping dependence [dashed line in Fig. 1(a)]. Through ¹⁷O-NMR measurements, it was concluded that this CDW could be static^{39,40} in origin. A similar short-range CDW was consistently found in Bi2201^{41,42}, Bi2212⁴³, Hg1201⁴⁴, and even in the electron-doped cuprate Nd_{2-x}Ce_xCuO₄⁴⁵. Recently, in Bi2201, a re-entrant incommensurate charge order with substantially long correlation lengths of 150-200 \AA that persists up to temperatures of at least 250 K was found in the high doping region, above which the pseudogap is closed ($p > 0.22$) [short-range CDW2 in Fig. 1(c)]⁴⁶.

Further high field RXS experiments on YBCO revealed that the CDW correlations in the CuO chain and between the CuO₂ planes are enhanced by $H \parallel c$, leading to a transition to a three-dimensional long-range CDW^{32,33}. These observations are consistent with the early discovery of a Fermi surface reconstruction by quantum oscillations⁴⁷ and a recent report of a thermodynamic phase transition in a high magnetic field⁴⁸.

C. Similarity and difference between YBCO and Bi2201

As described above, the RXS experiments suggested that the short-range CDW is widely observed in cuprates, indicating that the CDW is a new key ingredient to understanding the cuprate physics. By contrast, the long-range CDW order has only been found in YBCO and Bi2201. It was suggested that the CDWs in YBCO are related to its local structure, and that the periodic oxygen deficiency in the CuO chain (Ortho II/VIII structure⁴⁹) must be considered^{23,39}. Particularly, even at zero magnetic field, it was found that a long-range three dimensional CDW is induced by uniaxial pressure parallel to the CuO chain, rather than perpendicular to it, suggesting a strong correlation between the CuO chain and the CDWs in YBCO^{50,51}. Such a correlation with lattice distortion is also true for the stripe order in the La-based cuprate⁵².

By contrast, Bi2201 is a single-CuO₂-layer compound without a CuO chain, and exhibits no structural transitions. The CDW correlation is perfectly two-dimensional and limited to the CuO₂ plane⁴²; further, the temperature at which short-range CDWs occur in Bi2201 coincides with T^* ^{10,11,41,42}. Therefore, Bi2201 is of particular importance for the investigation of the CDWs. Moreover, the T_c^{max} of Bi2201 (= 32 K) is the lowest among the T_c^{max} values of cuprates, which allows us to study the doping evolution of the ground states without superconductivity. It is also a significant advantage of Bi2201 that a single crystal can be obtained in a wide doping range, from an underdoped antiferromagnetic insulator to an overdoped metal above the pseudogap end point [Fig. 1(c)].

III. NEW MEASUREMENTS AND RESULTS IN BI2201

Hereafter, we report new results of ^{63,65}Cu-NMR measurements of Bi2201 while reviewing the previous result²⁴. In the previous report, from the magnetic field and temperature dependence of the ⁶³Cu-NMR spectrum, we found that, for the doping level at which superconductivity begins to emerge, a field-induced CDW dominates over the spin order. Such CDW disappears before the superconductivity becomes optimum²⁴. Most importantly, we showed that T_{CDW} scales with T^* ²⁴. As new experimental results, here we demonstrate that the CDW appears regardless of whether the magnetic field is applied perpendicular or parallel to the CuO₂ plane. The anisotropy of the CDW is considerably smaller than that of H_{c2} . Furthermore, from systematic ⁶³Cu and ⁶⁵Cu nuclear spin lattice relaxation time (T_1) measurements, we find that both spin and charge fluctuations are present in the normal state even above T^* . The charge fluctuations become dominant in the doping regions where the field-induced CDW appears and at the pseudogap end point.

TABLE I: List of single crystals of Bi₂Sr_{2-x}La_xCuO_{6+δ}. $T_{\text{CDW}}^{H\perp c}$ and $T_{\text{CDW}}^{H\parallel c}$ indicate the onset temperature of the field-induced CDW order above $H \geq 13$ T. Some data are from our previous papers^{10,11,24}.

La(x)	p	T^* (K)	T_N (K)	T_c (K)	$T_{\text{CDW}}^{H\perp c}$ (K)	$T_{\text{CDW}}^{H\parallel c}$ (K)
0.90	0.093	250	140	–	–	–
0.80	0.107	240	66	–	–	–
0.75	0.114	230	–	12	60	48
0.65	0.128	210	–	19	50	44
0.60	0.135	195	–	20	35	30
0.55	0.142	190	–	23	30	25
0.50	0.149	175	–	23	18	12.5
0.40	0.162	160	–	32	–	–
0.15	0.198	65	–	22	–	–
0.10	0.205	60	–	19	–	–
0.08	0.208	45	–	14	–	–
0.04	0.213	30	–	10	–	–
0.00	0.219	–	–	8	–	–

Our results reveal that not only are the spin and charge orders of copper oxide intricately intertwined, but also their fluctuations, already in the normal state.

A. Samples

The single crystals of Bi₂Sr_{2-x}La_xCuO_{6+δ} listed in Table. 1 were grown by the traveling solvent floating zone method^{53,54}. The hole concentration (p) were estimated previously by the Hall coefficient⁵⁵. Small and thin single-crystal platelets, typically sized up to 2 mm-2 mm-0.1 mm, cleaved from an as-grown ingot, were used. The in-plane Cu-O bond direction (a or b axis) was determined by Laue reflection. $T_c(H)$ is defined as the onset temperature of diamagnetism observed by ac-susceptibility measurement using NMR coil²⁴.

B. NMR measurements

In Bi2201, there is only one Cu site in the single CuO₂ plane. For NMR measurements, the magnetic field is applied along the c ($H\parallel c$) and the Cu-O bond direction ($H\perp c$), respectively. The ⁶³Cu-NMR spectra were taken by sweeping the rf frequency at a fixed field. The data above $H = 15$ T were obtained by using the Hybrid magnet in the National High Magnetic Field Laboratory, Tallahassee, Florida²⁴.

For ^{63,65}Cu, the nuclear spin Hamiltonian is expressed as the sum of the Zeeman and nuclear quadrupole interaction terms, $\mathcal{H} = \mathcal{H}_z + \mathcal{H}_Q = -\gamma\hbar\mathbf{I} \cdot \mathbf{H}_0(1 + K) + (h\nu_Q/6)[3I_z^2 - I(I+1) + \eta(I_x^2 - I_y^2)]$, where gyromagnetic ratio $\gamma = 11.285$ MHz/T and $\gamma = 12.089$ MHz/T, K is the Knight shift, and $I = 3/2$ is the ^{63,65}Cu nuclear spin. The NQR frequency ν_Q and the asymmetry param-

eter η are defined as $\nu_Q = \frac{3eQV_{zz}}{2I(2I-1)\hbar}$, $\eta = \frac{V_{xx}-V_{yy}}{V_{zz}}$, with $^{63}Q = -0.211 \times 10^{-24} \text{ cm}^2$ and $^{65}Q = -0.195 \times 10^{-24} \text{ cm}^2$ and $V_{\alpha\beta}$ being the nuclear quadrupole moment and the electric field gradient (EFG) tensor⁵⁶. The principal axis z of the EFG is along the c axis and $\eta = 0$ ⁵⁷. Due to \mathcal{H}_Q , as shown in Fig. 2(a) and 2(b), one obtains the NMR center line and the two satellite transition lines between $|m\rangle$ and $|m-1\rangle$, ($|m\rangle = 3/2, 1/2$), at $\nu_{m \leftrightarrow m-1} = {}^{63,65}\gamma H_0(1+K) + (\nu_Q/2)(3\cos^2\theta - 1)(m-1/2) + \text{second-order correction}$ for ^{63}Cu and ^{65}Cu isotopes, respectively. Here, θ is the angle between \mathbf{H} and EFG. As shown in Fig. 2(c) and 2(d), in the antiferromagnetically ordered case below T_N and T_{CDW} , an internal field H_{int} and spatial distribution of δK and $\delta\nu_Q$ due to antiferromagnetic¹¹ and CDW^{24,58} orders appear to modify the spectrum shape, respectively.

The $^{63,65}\text{Cu}$ -NMR T_1 were measured at the center peak ($H\parallel c$) by using a single saturating pulse. To obtain T_1 , the recovery curve of nuclear magnetization was fitted by the theoretical function⁵⁹, $1 - M(t)/M_0 = 0.9\exp(-6t/T_1) + 0.1\exp(-t/T_1)$ where M_0 and $M(t)$ were the nuclear magnetization in the thermal equilibrium and at a time t after the saturating pulse. In strongly correlated electron systems, usually, T_1 probes the spin fluctuation through the hyperfine coupling constant $A_{\mathbf{q}}$ as ${}^{63,65}(1/T_1^M) \propto {}^{63,65}\gamma k_B T \sum_{\mathbf{q}} |A_{\mathbf{q}}|^2 \chi_{\perp}''(\mathbf{q}, \omega_0)/\omega_0$, where ω_0 is the NMR frequency⁶⁰ and \mathbf{q} is a wave vector for a spin order. In the case that T_1 probes the EFG fluctuation, then it is dominated by Q as ${}^{63,65}(1/T_1^Q) \propto 3(2I+3)({}^{63,65}Q^2)/[10(2I-1)I^2]$ ^{58,61}. Hence, the origin of T_1 can be identified from the ratio ${}^{65}(1/T_1)/{}^{63}(1/T_1)$, since ${}^{65}(1/T_1)/{}^{63}(1/T_1) = ({}^{65}\gamma/{}^{63}\gamma)^2 = 1.15$ when it is dominated by spin fluctuations and ${}^{65}(1/T_1)/{}^{63}(1/T_1) = ({}^{65}Q/{}^{63}Q)^2 = 0.85$ when it is governed by charge fluctuations.

C. Field and temperature dependence of the Cu-NMR spectrum

We observed the CDW order as a splitting of an NMR satellite peak due to in-plane EFG distribution²⁴. First, we show that this method is applicable even for the antiferromagnetic phase where H_{int} appears. As shown in Fig. 2(c) and 2(d), for a strongly underdoped antiferromagnetic insulator ($p = 0.107$), the low-temperature spectrum changes its shape due to H_{int} below $T_N = 66$ K, where $1/T_1T$ exhibits a peak [Fig. 2(e) and 2(f)]. However, the in-plane H_{int}^{\perp} is significantly smaller than the out-of-plane $H_{\text{int}}^{\parallel}$,¹¹ and thus, the satellite peaks for $H\perp c$ is almost unchanged across T_N . This allows us to verify the CDW even in the spin-ordered state.

Figures 3(a)-(e) show the temperature dependence of the ^{63}Cu -NMR satellite peak. The external magnetic field is $H\perp c = 13$ and 14.5 T. First, no change was observed for $p = 0.162$. For $p = 0.135$, however, the line width increased at $T = 4.2$ K. A splitting was also ob-

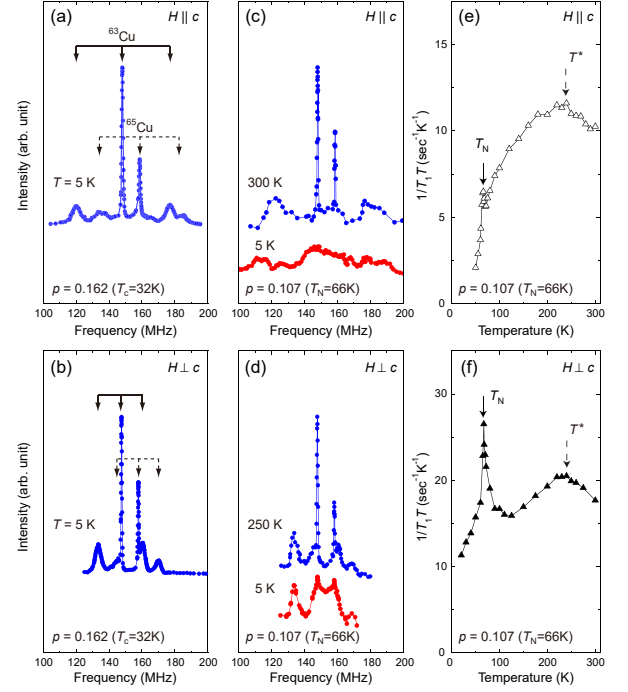


Fig. 2: $^{63,65}\text{Cu}$ -NMR spectrum of $p = 0.162$ at $T = 5$ K and that of $p = 0.107$ above and below T_N at $H = 13$ T obtained for $H\parallel c$ [(a) and (c)] and for $H\perp c$ [(b) and (d)], respectively. The lower satellite line ($3/2 \leftrightarrow 1/2$ transition) peak around 135 MHz was used for the detection of CDW for $H\perp c$. Temperature dependence of $1/T_1T$ of $p = 0.107$ in $H = 13$ T obtained for $H\parallel c$ (e) and for $H\perp c$ (f). Solid and dashed arrows indicate T_N and T^* .

served at $p = 0.128$ and 0.114 but disappeared for $p = 0.107$. As shown by the solid curves in the figure, the spectra for $p = 0.135, 0.128$, and 0.114 can be reproduced by a sum of two Gaussian functions by formulating the splitting as $\pm\delta f$.

To investigate the origin of the splitting, we focus on the results for $p = 0.114$, in which case δf is the largest. Figures 3(f) and 3(g) show the magnetic field and temperature dependence of the satellite line and $\delta f(T)$ under various magnetic fields. δf increases rapidly below $T_{\text{CDW}} = 30$ K, 55 K, and 60 K for $H = 11$ T, 13 T, and above 14.5 T, respectively. Figure 3(h) shows the magnetic field dependence of δf at $T = 4.2$ K. δf increases rapidly above $H_{\text{CDW}} = 10.4$ T and becomes constant above $H = 14.5$ T. Furthermore, as shown in Fig. 3(i), $1/T_1T$ shows a peak at $H = 13$ T below which δf starts to increase, although the peak is absent at $H = 9$ T. These results indicate that a magnetic-field-induced phase transition occurs at T_{CDW} above $H_{\text{CDW}} = 10.4$ T.

Next, we quantitatively show that this phase transition is due to charge ordering, but not a spin order. Figures 4(a) and 4(b) respectively show the satellite and center peaks, obtained above and below $T_{\text{CDW}} = 60$ K, at $H = 14.5$ T. Figure 4(c) shows the temperature dependence of the integrated intensity of each peak multiplied by

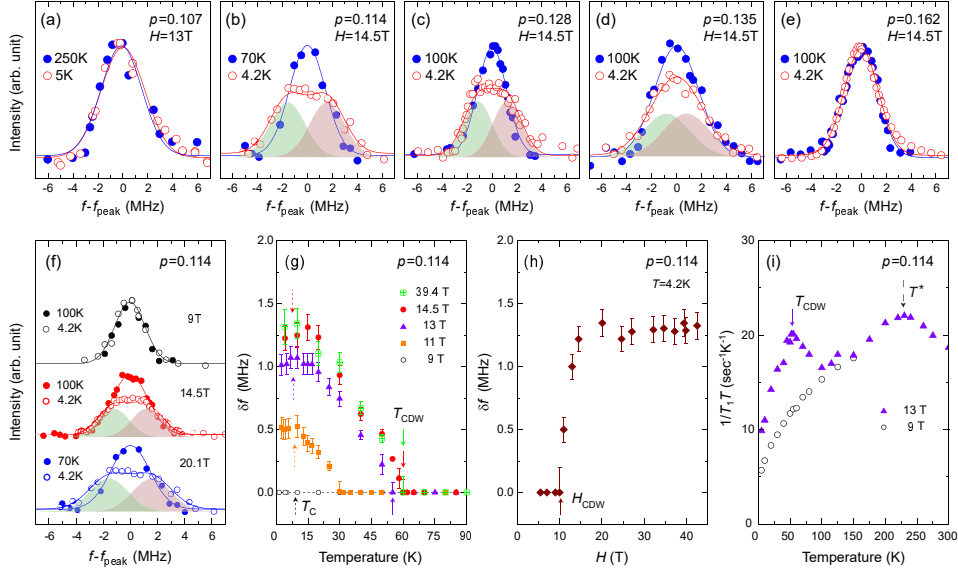


Fig. 3: (a-e) NMR satellite ($3/2 \leftrightarrow 1/2$ transition) lines for $\text{Bi}_2\text{Sr}_{2-x}\text{La}_x\text{CuO}_{6+\delta}$ with $p = 0.107, 0.114, 0.128, 0.135,$ and 0.162 . The curves for $p = 0.114, 0.128$ and 0.135 at $T = 4.2$ K are the sum of two Gaussian functions (shaded area). f_{peak} is the peak frequency. The intensity is normalized by the area of the spectrum. (f) Field and temperature dependence of the satellite line for $p = 0.114$. (g) Temperature evolution of δf for $p = 0.114$ under various fields. The solid arrows indicate T_{CDW} . The dotted arrows indicate $T_c(H)$. (h) Field evolution of the line splitting δf for $p = 0.114$ at $T = 4.2$ K. The solid arrow indicates H_{CDW} . (i) The temperature dependence of $1/T_1T$ at different fields. The solid arrow indicate T_{CDW} . The dashed arrow indicates T^* . Magnetic field is applied along the Cu-O bond direction ($H \perp c$).

temperature ($I \times T$), which is constant above T_c .

First, as shown in Fig. 2(d), in the case of the spin order, both the center and satellite lines become broader below T_N by the same amount ~ 0.4 MHz due to H_{int}^\perp . In contrast, as shown in Figs. 4(a) and 4(b), the satellite line becomes six times broader than the center line below T_{CDW} . Second, it is also different from the spin/charge-stripe order observed at $p = 0.125$ in the La-based cuprate²⁰. In Fig. 4(c), a reduction of $I \times T$, which is a characteristic of the stripe order, the so-called “wipe-out” phenomenon, is not observed. Further, in the stripe order, the spatial distribution of the localized spins causes a very large H_{int} distribution⁶², while the “split” of the spectrum below T_{CDW} shows evidence that the order parameter for the phase transition is spatially uniform. Finally, a magnetic-field-induced spin order was not found in our previous NMR experiments far above H_{c2} at $p = 0.162$ ⁶³.

These results indicate that the origin of the splitting of the spectra is not due to H_{int} , but the spatial periodic distribution of the Knight shift $K \pm \delta K$ and the NQR frequency $\nu_Q \pm \delta\nu$. Further, $\delta f_{\text{satellite}} = 1.22$ MHz is significantly larger than $\delta f_{\text{center}} = 0.271$ MHz, indicating that the origin is mainly ν_Q . Here, the parameters $\delta K = 0.05 \pm 0.01$ % and $\delta\nu = 2.5 \pm 0.2$ MHz can reproduce the two spectra simultaneously, as shown by the solid and dashed lines in Figs. 4(a) and 4(b)²⁴. In Bi2201, $\nu_Q = 22.0 + 39.6p$ was obtained²⁴, and from this, the spatial distribution of the hole concentration at the Cu site $\delta p = 0.06 \pm 0.01$ was determined. Therefore, we conclude

that the origin of δf is a magnetic-field-induced uniform charge distribution ($\delta p \sim 0.06$), i.e., the formation of the long-range CDW order below T_{CDW} .

D. Possible CDW structure in the CuO_2 plane

The “splitting” of the satellite peaks can be understood by the one-dimensional (1D) incommensurate CDW order in the CuO_2 plane. For the 1D CDW, the NQR frequency is distributed spatially as $\nu = \nu_Q + \delta\nu \cos(qX)$ ^{58,64}. X ($= a$ or b axis) is the modulation direction and $2\delta\nu$ ($\propto \delta f$) is the CDW order parameter^{58,64}. As a result, the spectrum exhibits a peak at $\nu = \nu_Q \pm \delta\nu$ [Fig. 4(d)]^{58,64}, and the Gaussian function reproduces the spectrum below T_{CDW} if an appropriate line width is given. Notably, although T_{CDW} shows similar values, the value of δp , that is, the amplitude of the CDW, is twice that for YBCO²³. This is because Bi2201 has a single CuO_2 plane, and the CDW correlation is limited to this plane⁴². Thus, it is considered that YBCO entails an effect of canceling out between its bi-layer CuO_2 planes³³. In YBCO, the magnetic field enhances the CDW correlation in the CuO chain and the coupling between the CuO_2 planes, resulting in a three-dimensional CDW order^{32,33}. By contrast, in Bi2201, the magnetic field yields a CDW^{41,42} with a 1D long-range order only limited in the CuO_2 plane.

The RXS experiment suggests a two-dimensional (2D) CDW with $\mathbf{Q} = (0.26, 0)$ and $(0, 0.26)$ and $\xi \sim 20\text{\AA}$ below

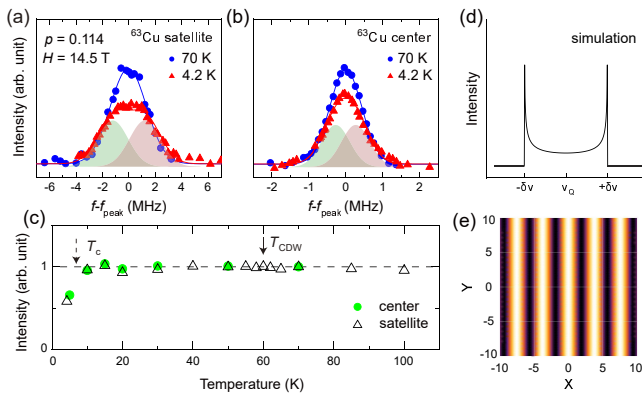


Fig. 4: Temperature dependence of satellite (a) and center (b) peaks of $p = 0.114$ sample obtained at $H_{\parallel} = 14.5$ T. The solid line is the fitting with a Gaussian function. The curve for $T = 4.2$ K is the sum of two Gaussian functions. (c) Temperature dependence of NMR intensities ($I \times T$) for the center (solid circles) and satellite (open triangles) peaks. Dotted and solid arrows indicate T_c ($H = 14.5$ T) and T_{CDW} , respectively. The decrease below T_c is due to the Meissner effect. (d) Frequency distribution of Cu-NMR spectrum reflecting the incommensurate charge distribution in the CuO_2 plane. (e) Schematic view of the spatial distribution of charges $\delta\nu\cos(qX)$ below $T = T_{CDW}$ in the CuO_2 plane. Yellow and black colors indicate $+\delta\nu$ and $-\delta\nu$, respectively. X and Y indicate the positions of Cu along the Cu-O bond directions.

T^* when $H = 0$ ^{42,65}. Furthermore, STM experiments on Bi2201 suggested a PDW with $\mathbf{q}_{PDW} = (0.25, 0)$ and $(0, 0.25)$ on the surface at low temperatures⁶⁶. In either case, if such a local CDW transforms to a long-range order, the spatial distribution of the NQR frequency will be $\nu = \nu_Q + \delta\nu_X \cos(qX) + \delta\nu_Y \cos(qY)$ ⁶⁴. When the CDW amplitudes are equivalent to $\delta\nu_X = \delta\nu_Y$, such CDWs yield $I(\nu) \sim -\ln[(\nu - \nu_Q)/\delta\nu]/\delta\nu$, resulting in a logarithmic singularity at $\delta\nu = 0$ ⁶⁴. Therefore, such a long-range 2D CDW order is not consistent with our results. However, if the amplitude in each direction is very different, $\delta\nu_{X(Y)} \gg \delta\nu_{Y(X)}$ or there are CDW domains with modulations $\nu_X = \nu_Q + \delta\nu_X \cos(qX)$ and $\nu_Y = \nu_Q + \delta\nu_Y \cos(qY)$ in each domain, the NMR lineshape will be the same as that for the 1D CDW. Figure 4 (e) schematically shows the spatial modulation of the NQR frequency, $\delta\nu\cos(qX)$, by assuming that a short-range CDW with $\mathbf{Q} = (0.26, 0)$ ⁶⁵ becomes a long-range order under a magnetic field.

E. Relationship between CDW and superconductivity

To clarify the relationship between the CDW and superconductivity in more detail, we investigated the anisotropy of the CDW. Figure 5(a) shows the doping dependence of the CDW order in $H_{\parallel} c = 13$ T determined by the temperature dependence of $1/T_1 T$ ²⁴. Figure 5(b)

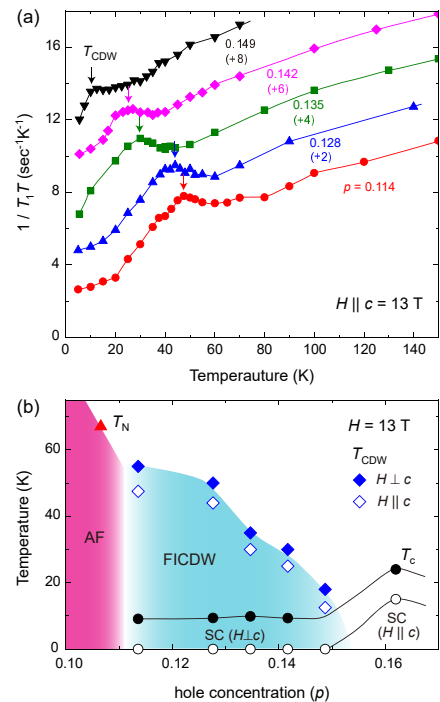


Fig. 5: (a) Temperature dependence of $1/T_1 T$ for $p = 0.114$ to 0.149 obtained at $H_{\parallel} c = 13$ T. The data is offset for clarity. Arrows indicate T_{CDW} . (b) Phase diagram of antiferromagnetism (AF), FICDW, and superconductivity (SC) at $H = 13$ T. T_c s are from ref²⁴.

shows the phase diagram of antiferromagnetism, CDW, and superconductivity in $H = 13$ T. The anisotropy of the CDW is considerably smaller than that of the upper critical field for the superconductivity²⁴. Therefore, vortices are not involved in the origin of CDWs. Rather, our results suggest that the CDW and superconductivity can coexist²⁴. This conclusion is supported by a more recent work for YBCO with $H_{\parallel} c$ ⁶⁷.

F. Relationship between CDW, antiferromagnetism, and pseudogap

In this subsection, we summarize the relationship between CDW and other phenomena. First, $T_N = 66$ K for $p = 0.107$ appears to be smoothly replaced by $T_{CDW} = 60$ K for $p = 0.114$ where superconductivity appears. This indicates that CDW is more likely to be induced at the border of antiferromagnetism than at $p \sim 1/8$. Here, the pseudogap ground state of $p \geq 0.114$ is a metallic state with a finite density of states^{10,11}. Therefore, the degree of freedom of charge is as important as that of spin in the development of high-temperature superconductivity. Second, the CDW is suppressed with increasing hole doping and disappears before the optimum T_c is reached at $p = 0.162$. Most importantly, as shown in Fig. 6, we find that T_{CDW} and T^* have a positive correlation for the

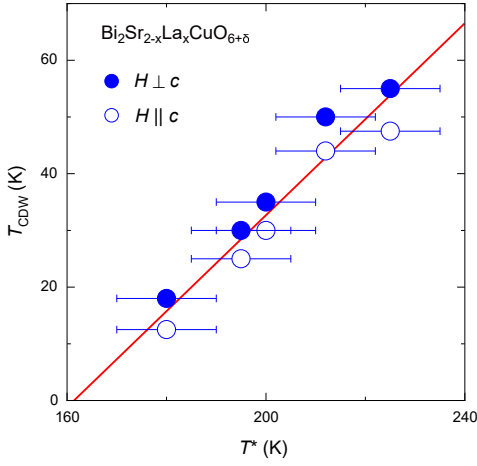


Fig. 6: A plot of T_{CDW} vs T^* at $H = 13$ T. The straight line is a linear fitting to the data, which yields a slope of 0.9 ± 0.1 . Error bars represent the uncertainty in defining T^* .

entire doping range. Because no static order is observed at T^* by NMR, Fig. 6 suggests that T^* is attributable to the CDW (charge) fluctuation as discussed in the next subsection. Polar Kerr effect¹⁶ and optical conductivity measurements⁶⁸ have suggested a symmetry breaking at T^* . Note that, however, the timescales of these experiments are several orders of magnitude faster than NMR time scale. In view of this difference, these results may be consistent since T^* may appear as a crossover in probes with a slower time windows.

G. CDW fluctuations

In this subsection, we report the results of the spin/charge fluctuations in the CuO_2 plane through the $^{63,65}\text{Cu}$ NMR magnetic/quadrupolar relaxation. Figures 7(a)-(c) show the recovery curves of ^{63}Cu and ^{65}Cu nuclear magnetization obtained at $T = 300$ K for the antiferromagnetic insulator with $p = 0.107$, CDW metal with $p = 0.114$, and superconductor with $p = 0.162$, respectively. A magnetic field $H = 13$ T was applied along the c axis. First, both $^{63,65}\text{Cu}$ nuclear magnetization curves for $p = 0.107$ and 0.162 are the same [$^{65}(1/T_1)/^{63}(1/T_1) = 1$], indicating that the relaxation process entails a mixture of spin and charge fluctuations in the normal state, regardless of the antiferromagnetic insulator or superconductors. In contrast, we observed a longer T_1 for ^{65}Cu than for ^{63}Cu at $p = 0.114$, which yields $^{65}(1/T_1)/^{63}(1/T_1) = 0.85$, i.e., charge fluctuations are dominant in the normal state of the CDW ordered phase.

Early NMR studies on polycrystalline YBCO^{69,70} have suggested that the spin fluctuation was predominant and there was no charge fluctuation in the CuO_2 plane. However, our results show that in addition to spin fluctuations, charge fluctuations are active in the CuO_2 plane.

We summarize the relationship between spin/charge

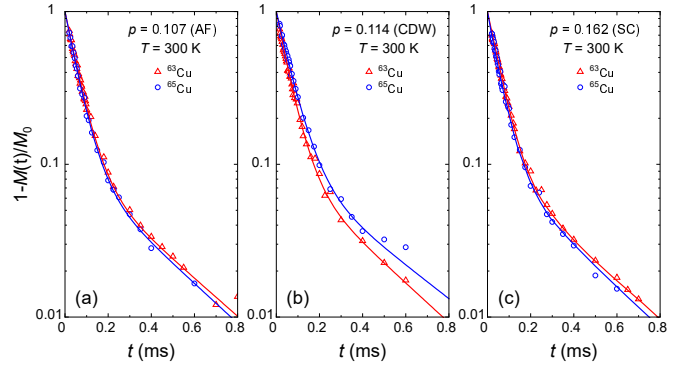


Fig. 7: Typical recovery curves of the nuclear magnetization for ^{63}Cu and ^{65}Cu obtained at $T = 300$ K for $p = 0.107$ (a), 0.114 (b), and 0.162 (c). Solid curves are fits to the theoretical formula, $1 - M(t)/M_0 = 0.9\exp(-6t/T_1) + 0.1\exp(-t/T_1)$ ⁵⁹.

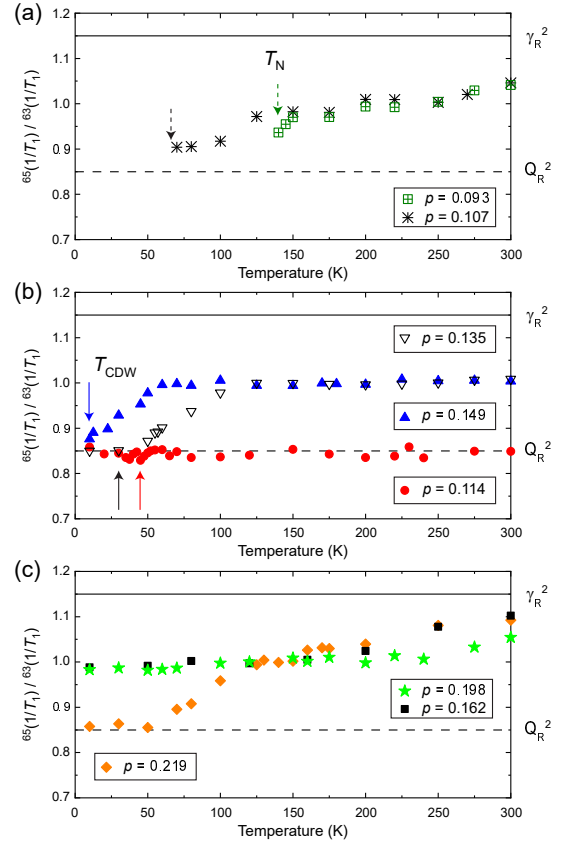


Fig. 8: Temperature dependence of the ratio $^{65}(1/T_1)/^{63}(1/T_1)$ for strongly-underdoped antiferromagnets (a), underdoped CDW ordered superconductors (b), and overdoped superconductors (c) obtained at $H = 13$ T parallel to the c axis. Solid and dotted arrows indicate T_{CDW} and T_N , respectively. Solid and dashed horizontal straight lines indicate the values expected for the magnetic relaxation process [γ_R^2 ($= 1.15$)] and for the quadrupole relaxation process [Q_R^2 ($= 0.85$)], respectively.

order and fluctuations and pseudogap in Bi2201. Figures 8(a)-(c) show the temperature dependence of the ratio $^{65}(1/T_1)/^{63}(1/T_1)$ for strongly underdoped antiferromagnets with $p = 0.093$ and 0.107 [Fig. 8(a)], underdoped CDW-ordered superconductors with $0.114 \leq p \leq 0.149$ [Fig. 8(b)], and overdoped superconductors with $0.162 \leq p \leq 0.219$ [Fig. 8(c)]. Figure 9 shows the phase diagram for Bi2201, including the information on fluctuations in $H \parallel c = 13$ T. T_N , T_{CDW} , $T_c(H = 0)$, and T^* with respect to La (x) and the hole concentration (p) are plotted with the magnitude of the T_1 ratio indicated by color. Spin and charge fluctuations are both present above T_N in the antiferromagnetic insulators ($p = 0.093$ and 0.107). Notably, for $p = 0.114$, where T_{CDW} is the highest, the charge fluctuation dominates over the entire temperature range. With increasing doping, both the spin and charge fluctuations come into play again for $p = 0.135$ and 0.149 superconductors with the charge fluctuations dominating below T^* . The charge fluctuations becomes less notable, but persist along with spin fluctuations as the CDW order disappears in the superconductors with $p = 0.162$ and 0.198 .

Another surprising behavior was observed in the heavily overdoped superconductor with $p = 0.219$, above which the pseudogap closes ($T^* = 0$). A mixture of spin and charge fluctuations is still visible at $p = 0.219$, but spin fluctuation is dominant above $T = 250$ K. As the temperature is lowered, the spin fluctuation is reduced and the charge fluctuation becomes dominant below $T = 50$ K, although the CDW order is *absent* at $p = 0.219$. We note that a stripe ordering below $T = 80$ K has been found in the La-based cuprate at $p = 0.21$, which was suggested by neutron scattering experiment to be derived from spin fluctuations²¹. However, spin fluctuation is not noticeable in Bi2201. Therefore, our observation at the pseudogap end point in Bi2201 is not related to the stripe ordering.

IV. DISCUSSION

Our results revealed that charge fluctuations coexist with spin fluctuations over the entire doping range from high temperatures above T^* to low temperatures where superconductivity occurs. This supports the suggestion that the T^* is associated with the charge fluctuation. In contrast, at high temperatures and heavily overdoped regions away from the pseudogap, the spin fluctuation dominates over the charge fluctuation (orange region in Fig. 9).

In two regions near the endpoints of the superconducting dome, the charge fluctuation dominates. The first one is the region where field-induced CDWs occur. The charge fluctuation dominates the spin fluctuation at the border of antiferromagnetism. This is in good agreement with the replacement of T_{CDW} with T_N . The other is at the pseudogap end point around $p \sim 0.22$. These results are qualitatively consistent with X-ray measurements at

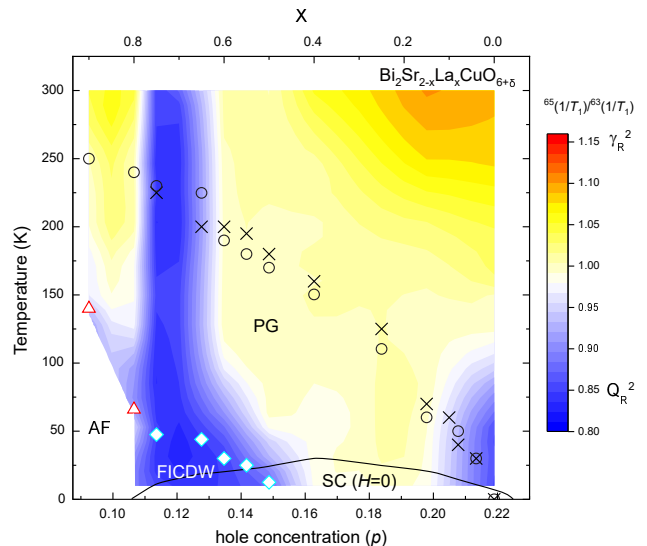


Fig. 9: Carrier concentration dependence of pseudogap (PG), antiferromagnetism (AF), field-induced CDW (FICDW), and superconductivity [SC ($H = 0$)] for $\text{Bi}_2\text{Sr}_{2-x}\text{La}_x\text{CuO}_{6+\delta}$. The color coding (bar on right) refers to the ratio $^{65}(1/T_1)/^{63}(1/T_1)$. Red, blue, and yellow shadings indicate the spin, charge, and mixed fluctuations, respectively. Open triangles, diamonds, and circles (crosses) indicate T_N , T_{CDW} , and T^* , respectively. Solid curve indicates T_c at $H = 0$. $\gamma_R^2 = 1.15$ and $Q_R^2 = 0.85$ are indicated on the bar, respectively.

$H = 0$ [Fig. 1(c)]^{41,42,46,65}. The origin of the charge fluctuation in the two different regions, however, may be different. The former is a precursor to the CDW order. In the latter case, it is probably due to quantum critical fluctuations around the pseudogap endpoint. In fact, a growth of nematic susceptibility or specific heat was observed in several compounds at the pseudogap end point⁷¹⁻⁷³.

Finally, a nematic order was recently reported in the pseudogap regime by torque magnetometry on $\text{YBa}_2\text{Cu}_3\text{O}_y$ ⁷⁴ and by ^{17}O -NMR experiments on $\text{YBa}_2\text{Cu}_4\text{O}_8$ ⁴⁰. The relationship and interplay between CDW orders/fluctuations and nematicity await future studies. Also, experiments at different time/length scales and magnetic-field dependence are important to further investigate the role of charge.

V. SUMMARY

We reviewed the CDW orders in $\text{Bi}_2\text{Sr}_{2-x}\text{La}_x\text{CuO}_{6+\delta}$ with comparison to YBCO and Bi2212, and presented our new NMR results on the CDW order and fluctuations. We clarified the relationship between spin/charge dynamics/orders and pseudogap. We find that the CDW appears, regardless of the magnetic field parallel or perpendicular to the CuO_2 plane. However, the anisotropy of the CDW is considerably smaller than that of H_{c2} .

The CDW takes over the spin order in the region $p \geq 0.114$ and coexist with superconductivity, but disappears before the optimal doping level is reached. We find T_{CDW} scales with T^* . The charge fluctuations coexist with spin fluctuations in the CuO_2 plane in the entire doping and temperature regions, but are dominant in the two end regions of the superconducting dome. In the first region with $0.114 \leq p \leq 0.149$, the field-induced CDW order appears, while in the second region where the pseudogap

ends, charge fluctuations show up. These results demonstrate the usefulness of NMR in research on both static and dynamic properties, and hopefully will provide some hints for the future research in cuprates.

We would like to thank Z. Li, M. Kitahashi, P. L. Kuhns, and A. P. Reyes for contribution in the early part of this work, and T. Tohyama for discussion. This work was supported in part by research grants from MEXT (Nos. JP19K03747 and JP19H00657).

-
- ¹ J. G. Bednorz and K. A. Müller, *Z. Phys.* **64**, 189 (1986).
² B. Keimer *et al.*, *Nature* **518**, 179 (2015).
³ C. C. Tsuei and J. R. Kirtley, *Rev. Mod. Phys.* **72**, 969 (2000).
⁴ J. Bardeen, L. N. Cooper, and J. R. Schrieffer, *Phys. Rev.* **108**, 1175 (1957).
⁵ A. Schilling *et al.*, *Nature* **363**, 56 (1993).
⁶ P. A. Lee, N. Nagaosa, and X. -G. Wen, *Rev. Mod. Phys.* **78**, 17 (2006).
⁷ T. Timusk and B. Statt, *Rep. Prog. Phys.* **62**, 61 (1999).
⁸ H. Yasuoka, T. Imai, and T. Shimizu, *Strong Correlation and Superconductivity*, ed. H. Fukuyama, S. Maekawa, and A. P. Malozemoff (Springer-Verlag, New York, 1989) p. 254.
⁹ H. Alloul, T. Ohno, and P. Mendels, *Phys. Rev. Lett.* **63**, 1700 (1989).
¹⁰ G.-q. Zheng *et al.*, *Phys. Rev. Lett.* **94**, 047006 (2005).
¹¹ Shinji Kawasaki *et al.*, *Phys. Rev. Lett.* **105**, 137002 (2010).
¹² D. S. Marshall *et al.*, *Phys. Rev. Lett.* **76**, 4841 (1996).
¹³ H. Ding *et al.*, *Nature* **382**, 51 (1996).
¹⁴ A. G. Loeser *et al.*, *Science* **273**, 325 (1996).
¹⁵ M. R. Norman *et al.*, *Nature* **392**, 157 (1998).
¹⁶ R. -H. He *et al.*, *Science* **331**, 1579 (2011).
¹⁷ S. Straßle *et al.*, *Phys. Rev. Lett.* **106**, 097003 (2011).
¹⁸ A. M. Mounce *et al.*, *Phys. Rev. Lett.* **111**, 187003 (2013).
¹⁹ J. Crocker *et al.*, *Phys. Rev. B* **84**, 224502 (2011).
²⁰ J. M. Tranquada *et al.*, *Nature* **375**, 561 (1995).
²¹ Y. Koike *et al.*, *Physica C* **364-365**, 562 (2001).
²² A. Himeda, T. Kato, and M. Ogata, *Phys. Rev. Lett.* **88**, 117001 (2002).
²³ T. Wu *et al.*, *Nature* **477**, 191 (2011).
²⁴ S. Kawasaki *et al.*, *Nat. Commun.* **8**, 1267 (2017).
²⁵ J. E. Hoffman *et al.*, *Science* **295**, 466 (2002).
²⁶ T. Zhang, E. Demler, and S. Sachdev, *Phys. Rev. B* **66**, 094501 (2002).
²⁷ S. A. Kivelson *et al.*, *Phys. Rev. B* **66**, 144516 (2002).
²⁸ Daniel F. Agterberg *et al.*, *Annu. Rev. Condens. Matter Phys.* **11**, 231 (2020).
²⁹ T. Tohyama, *Jpn. J. Appl. Phys.* **51**, 010004 (2011).
³⁰ Patrick A. Lee, *Phys. Rev. X* **4**, 031017 (2014).
³¹ E. Fradkin, S. A. Kivelson, and J. M. Tranquada, *Rev. Mod. Phys.* **87**, 457 (2015).
³² S. Gerber *et al.*, *Science* **350**, 949 (2015).
³³ J. Chang *et al.*, *Nat. Commun.* **7**, 11494 (2016).
³⁴ T. Wu *et al.*, *Nat. Commun.* **4**, 2113 (2013).
³⁵ J. A. Lee *et al.*, *New. J. Phys.* **19**, 033024 (2017).
³⁶ G. Ghiringhelli *et al.*, *Science* **337**, 821 (2012).
³⁷ J. Chang *et al.*, *Nature Phys.* **8**, 871 (2012).
³⁸ M. Takigawa *et al.*, *Phys. Rev. B* **43**, 247 (1991).
³⁹ T. Wu *et al.*, *Nat. Commun.* **6**, 6438 (2015).
⁴⁰ W. Wang *et al.*, *Sci. China-Phys. Mech. Astron.* **64**, 237413 (2021).
⁴¹ R. Comin *et al.*, *Science* **343**, 390 (2014).
⁴² Y. Y. Peng *et al.*, *Phys. Rev. B* **94**, 184511 (2016).
⁴³ E. H. da Silva Neto *et al.*, *Nat. Commun.* **5**, 5875 (2014).
⁴⁴ W. Tabis *et al.*, *Nat. Commun.* **5**, 5875 (2014).
⁴⁵ E. H. da Silva Neto *et al.*, *Science* **347**, 282 (2015).
⁴⁶ Y. Y. Peng *et al.*, *Nature Mater.* **17**, 697 (2018).
⁴⁷ N. Doiron-Leyraud *et al.*, *Nature* **447**, 565 (2007).
⁴⁸ D. LeBoeuf *et al.*, *Nature Phys.* **9**, 79 (2013).
⁴⁹ N. H. Andersen *et al.*, *Physica C* **317-318**, 259 (1999).
⁵⁰ M. Bluschke *et al.*, *Nat. Commun.* **9**, 2978 (2018).
⁵¹ H.-H. Kim *et al.*, *Science* **362**, 1040 (2018).
⁵² J. D. Axe *et al.*, *Phys. Rev. Lett.* **62**, 2751 (1989).
⁵³ J. B. Peng and C. T. Lin, *J. Supercond. Nov. Magn.* **23**, 591 (2010).
⁵⁴ B. Liang and C. T. Lin, *J. Cryst. Growth* **267**, 510 (2004).
⁵⁵ S. Ono *et al.*, *Phys. Rev. Lett.* **85**, 638 (2000).
⁵⁶ A. Abragam, *The principles of nuclear magnetism* (Oxford University Press, London, 1961).
⁵⁷ G.-q. Zheng *et al.*, *J. Phys. Soc. Jpn.* **64**, 2524 (1995).
⁵⁸ S. Kawasaki *et al.*, *Phys. Rev. B* **91**, 060510(R) (2015).
⁵⁹ A. Narath, *Phys. Rev.* **162**, 320 (1967).
⁶⁰ T. Moriya, *J. Phys. Soc. Jpn.* **18**, 516 (1963).
⁶¹ Y. Obata, *J. Phys. Soc. Jpn.* **19**, 2348 (1964).
⁶² A. W. Hunt *et al.*, *Phys. Rev. B* **64**, 134525 (2001).
⁶³ J.-W. Mei *et al.*, *Phys. Rev. B* **85**, 134519 (2012).
⁶⁴ R. Blinc and T. Apih, *Prog. Nucl. Magn. Reson. Spectrosc.* **41**, 49, (2002).
⁶⁵ R. Comin *et al.*, *Nature Mater.* **14**, 796 (2015).
⁶⁶ K. Fujita *et al.*, *PNAS* **111**, E3026 (2014).
⁶⁷ J. Kačmarčík *et al.*, *Phys. Rev. Lett.* **121**, 167002 (2018).
⁶⁸ L. Zhao *et al.*, *Nature Phys.* **13**, 250 (2017).
⁶⁹ Y. Kitaoka *et al.*, *J. Phys. Soc. Jpn.* **57**, 30 (1988).
⁷⁰ T. Imai *et al.*, *J. Phys. Soc. Jpn.* **57**, 1771 (1988).
⁷¹ K. Ishida *et al.*, *J. Phys. Soc. Jpn.* **89**, 064707 (2020).
⁷² C. Girod *et al.*, *Phys. Rev. B* **103**, 214506 (2021).
⁷³ M. Lizaire *et al.*, *Phys. Rev. B* **104**, 014515 (2021).
⁷⁴ Y. Sato *et al.*, *Nature Phys.* **13**, 1074 (2017).